JOURNAL OF MATERIALS SCIENCE 2 (1967) 538–558

A Study on Orientation Effects in Polyethylene in the Light of Crystalline Texture

Part 2 *Correlation of the Molecular Orientation with that of the Textural Elements*

I. L. HAY, A. KELLER
H. H. Wills Physics Laboratory, The University, Bristol, UK

Received 26 May 1967

The experiments and their interpretation presented here examine the interrelation between the crystalline and amorphous components of oriented polymers. In particular, oriented low-density polyethylene was examined by low-angle X-ray scattering in successive stages of heat relaxation, both at room temperature and at the temperature of the heat-treatment. These experiments were supplemented by measurements of dimensional changes occurring during annealing and those produced by swelling. The effect of redrawing from various stages of annealing and that of oxidation on the orientation behaviour were also examined. The results were correlated with the molecular orientation behaviour established by wide-angle X-ray diffraction in part 1 [1]. According to the picture which emerges, the oriented material consists of lamellae, established during the earliest stages of annealing, having $\{h0l\}$ basal planes, in close analogy with the unoriented bulk-grown and appropriate solution-grown crystals. The first stages of the reorientation process on annealing consist of interlamellar slip, activated by a uniaxial compression released by the heat-treatment. Such slip also characterises the corresponding stages of redrawing, providing an example of a definitive textural process which ought also to occur under more general conditions of drawing. The present evidence points to definitive individuality of the lamellae, which suggests at least a certain amount of chain-folding. The later stages of reorientation occur by intralamellar slip which conforms to the established crystal plasticity elements. At progressively higher annealing temperatures, increasing melting takes place leading to oriented recrystallisation on cooling. The resulting orientation conforms to that expected from crystallisation emanating from strings of nuclei which persist after all crystalline material has melted, pointing to important analogies with crystallisation under stress [13]. This recrystallisation may also be influenced by uniaxial pressure which could persist in samples not yet fully relaxed. In addition to the compressive forces, forces which tend to restore the initial orientation are manifest. The latter are likely to be generated by the slip processes themselves. This points to different kinds of amorphous material distinguished by their relation to the crystalline morphology.

Erratum to Part 1 [1]
Page 45, column 1, lines 39-40 (last two lines of third paragraph) should read: "where a, b, and c axes are along x, z, and y axes respectively."

1. Introduction

In part 1 [1], a detailed study of the molecular reorientation, which occurs when drawn polyethylene is annealed, was reported. It was shown

there, by using drawn and rolled material, that the changes follow a progressive sequence up to the melting point, thus resolving some anomalies in earlier studies [2, 3]. This sequence was deduced mainly from wide-angle X-ray diffraction studies and a summary of the results is included here for reference purposes (figs. 1pw-8pw and table I). Such a sequence implies that some underlying textural changes are occurring within the sample. To look for these, low-angle X-ray diffraction studies were made on the same samples as used before [1]. The results of this study are reported here with some supplementary observations on similar drawn and rolled samples. These latter include X-ray diffraction at the annealing temperatures, redrawing of annealed samples, the effect of swelling agents, and nitric acid degradation studies. By correlating these results with the molecular orientations [1], a picture of the structural changes occurring during the full range of annealing, and to a lesser extent during some stages of drawing, is developed. Direct observations on the morphology will not be reported here. Work on this aspect is now in progress [4], and it is hoped that this will form the continuation of the series.

2. Experimental

2.1. Instrumental and Samples

The preparation of the drawn, rolled, and annealed samples was described in part 1 [1]. The notation for the directions is redefined in fig. 11. The annealing sequence will be characterised by the temperature, and the various properties to be measured will be presented as a function of the annealing temperature. It should be noted, however, that the dimensions of the specimens and the rate of heating will somewhat affect the temperature at which a particular stage of annealing, as assessed say by the low-angle X-ray patterns, is realised. Unless otherwise stated, all the experiments to be presented here were carried out on samples annealed under identically defined conditions, consequently the different measurements will be comparable when referred to the same annealing temperature. The temperature scale therefore serves essentially

TABLE I Summary of the changes in the wide- and low-angle X-ray diffraction with increasing relaxation temperature.

Range	Relaxation temperature (° C)	Wide-angle X-ray diffraction effects	Low-angle X-ray diffraction effects
1	60 70	Loss of (1 1 0) twin orientation First single crystal (stage A, fig. 2pw)	Intensification of reflections Reflections lie in the xy plane (fig. 2pL); the basal plane of lamellae is {3 0 1} (fig. 2m)
2	75	Gradual tilting of chains around **b** (figs. 3pw and 4pw)	Correlated rotation of chains and lamellae, by interlamellar slip, bringing the lamellae normal to y (stage B, figs. 4pL and 4m); in the final stage, there is a crystal transformation, decreasing the obliquity to {2 0 1}
3	105	Tilting of chains around **b** continued (fig. 5pw)	Lamellae remain normal to y, intralamellar slip occurs increasing the obliquity (figs. 5pL and 5m)
4	108	Tilting continued until **c** parallel to x (stage C, fig. 7pw)	Disruption of lamellae and re-establishment with a distribution centred on x (figs. 7pL and 7m)
5	110	Disorientation of chains around z Spherulite fibril analogue (stage D, fig. 8pw)	Disorientation of $\mathbf{n}_L$ in the xy plane Full randomisation of $\mathbf{n}_L$ around z (fig. 8pL)
6	115	Complete randomisation of chains	Complete randomisation of $\mathbf{n}_L$

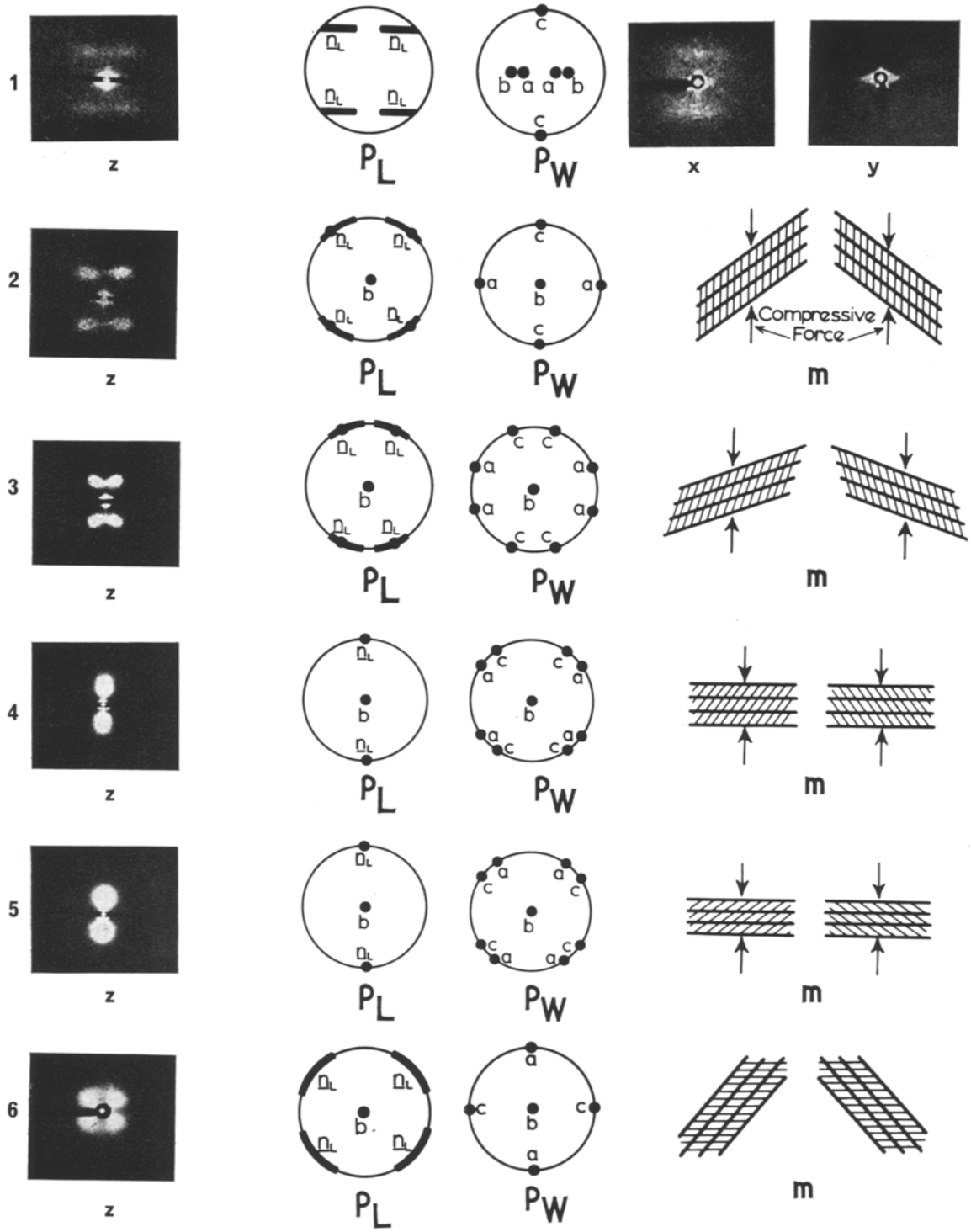
1
z
P_L
c
b a a b
c
P_W
x
y
2
z
P_L
c
a b a
c
P_W
Compressive Force
m
3
z
P_L
c c
a a
a b a
c c
P_W
m
4
z
P_L
c c
a a
b
a a
c c
P_W
m
5
z
P_L
a a
c c
b
c c
a a
P_W
m
6
z
P_L
a
c b c
a
P_W
m

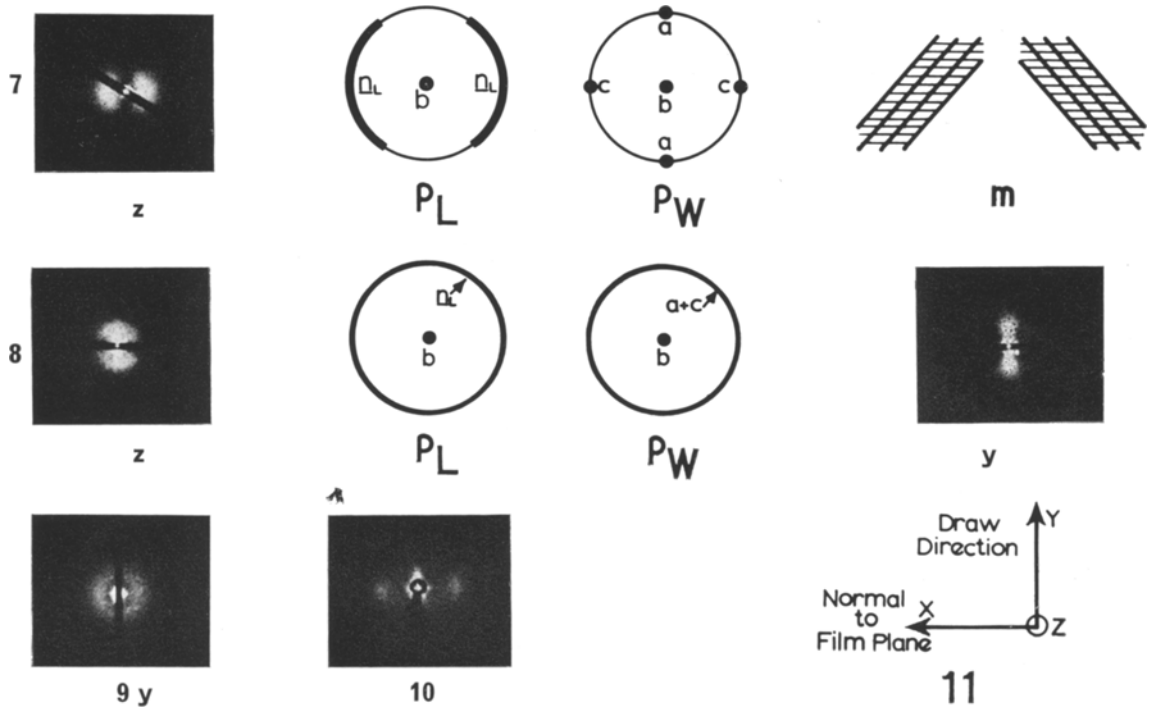

Figures 1 to 9 X-ray diffraction results on drawn and rolled, high-pressure polyethylene for various relaxation temperatures: (fig. 1) unrelaxed; (2) 70° C (stage A – approximation specified in part 1 [1]); (3) 95° C (range 2); (4) 105° C (stage B); (5) 107° C (range 3); (6) 110° C; (7) 110° C (stage C); (8) 113° C (stage D); (9) 116° C (random). Figs. z, x, and y are low-angle diffraction patterns, the notation referring to the specimen direction parallel to the X-ray beam (see fig. 11). *y* is vertical in figs. z and x, *x* is vertical in fig. y. (Note that a trace of the direct beam, in the shadow of the back stop, appears at the centre of each pattern.)

The notations p_L and p_W refer to idealised pole-figures for the low- and wide-angle orientations respectively, where *z* is normal to the plane of the drawing and *y* vertical.

The notation m refers to lamellar models for the textures represented by p_L and p_W (the fine striations represent the molecular direction).

Figure 10 Low-angle X-ray diffraction from a sample relaxed at 75° C. (X-rays at 40° to *x*; *z* vertical.)

Figure 11 Diagram to define the macroscopic axes.

only as a labelling of the specimens and has no absolute significance; the individual temperature figures will not be utilised as such.

The low-angle camera used was a Franks type [5] giving a focused, point-collimated beam. Point collimation is essential for the present work as it ensures that the azimuthal position of the maxima is faithfully reproduced, a prerequisite of orientation studies.

Some of the diffraction patterns were recorded at elevated temperatures. This was achieved with an oven arrangement (due to P. J. Holdsworth in this laboratory) adaptable to both wide- and low-angle cameras. Temperature control was better than $\pm\frac{1}{2}$° C.

The particulars of the swelling and the nitric acid degradation experiments will be quoted in the relevant sections.

2.2. Low-Angle X-ray Studies

2.2.1. Interpretation of the Low-Angle X-ray Patterns

The low-angle X-ray patterns from polymers cannot be interpreted with precision in molecular terms owing to their poor definition and the lack of higher orders. The observation of discrete diffraction only indicates that there is an electron density fluctuation on the scale of 100 Å. A more concrete model requires information from other sources to be invoked, as mentioned in section 1 of part 1. It was stated there that an accumulation of evidence suggests that the textural elements responsible for the low-angle reflections are of lamellar nature. For convenience in description, we shall refer to our low-angle X-ray results as due to lamellae, recognising that conclusive evidence for this does not come from X-ray studies alone.

Two kinds of basic information are directly derivable from the low-angle diffraction patterns. The first is the direction, the second the scale of the electron density fluctuation, which in terms of the lamellar morphology would correspond to the orientation and the thickness of the lamellae respectively. The orientation is our principal concern in this work. In a given photograph, it is directly defined by the azimuthal position of the discrete low-angle maximum; we identify the corresponding reciprocal lattice vector with the lamellar normal which we denote by $\mathbf{n}_L$ in what follows. Of course, a single photograph only gives one section of reciprocal space. In the region of small angles, this is practically a plane section passing through the origin of reciprocal space perpendicular to the X-ray beam. In the absence of fibre symmetry, this is inadequate to define the maximum in the $\mathbf{n}_L$ pole distribution. As in the case of the wide-angle patterns (part 1), therefore, photographs were taken with the beam along each of the three principal directions (x, y, z) of the specimen. This, together with occasional intermediate positions for check, was found to be an adequate substitute for continuous mapping, in view of the fact that the orientation distribution found was particularly clear-cut. The second quantity, the scale of the lamellar periodicity, is of lesser importance for this work and will be commented on later.

The low-angle results recorded at room temperature are illustrated in figs. 1-9. They show that both the lamellar orientation and the spacing vary with the annealing temperature. These two effects will be discussed separately.

2.2.2. Changes in Lamellar Orientations

The orientation changes in the low-angle patterns divide the annealing sequence into several distinct ranges as summarised in table I. The results will be presented according to this division. Comparison with the wide-angle patterns is afforded by the third column in table I and by the pole figures of figs. 1p_W-8p_W. The latter can be compared with the pole figure representation of the low-angle reflections ($\mathbf{n}_L$ poles) as seen along the corresponding (z) projection (figs. 1p_L-8p_L). The definition of the axes is given by fig. 11.

Range 1 The low-angle pattern before rolling is not illustrated as it is the familiar layer-line streak with some off-meridional intensifications (four-point diagram – e.g. [6]) and with fibre symmetry. On rolling, the fibre symmetry is lost (figs. 1x, y, z). A four-point effect with a split of about $\pm 45°$ about y is still seen with the beam along z (fig. 1z), but fig. 1x only shows an indefinite pattern centred on the draw direction. No pattern is observed with the beam along the draw direction (fig. 1y), in common with the drawn-only material and with all the subsequent annealing stages up to that in fig. 7.

Slight annealing, which in the wide-angle patterns produces the first single-crystal analogue (fig. 2p_W – stage A, see part 1), enhances this asymmetry. It results in a clearly defined double texture (fig. 2z – no reflections with the beam along x or y) where the two sets of lamellar normals, hence $\mathbf{n}_L$ poles, are concentrated in the xy plane split by 45° about y. This means that the lamellae are parallel to z and inclined through 45° to y. This assignment is further confirmed on a sample where the split was $\pm 40°$ (i.e. intermediate between figs. 2 and 3 – see below) with a beam normal to z but at 40° to x. In the resulting pattern (fig. 10), a pair of reflections is seen on the direction perpendicular to z, as expected if the $\mathbf{n}_L$ poles were confined to the xy plane.

All through the rest of the annealing series, z remains the zone axis for the lamellae, consequently only photographs taken along z will be illustrated for the successive stages.

Range 2 As seen from figs. 3z and 4z, the maxima move towards y on increasing the annealing temperature, until they finally coalesce there (figs. 4z-5z). The spread along layer lines

perpendicular to y shown by fig. 2z, however, is not retained. Each low-angle maximum is spread obliquely to y as sketched in fig. 12. They

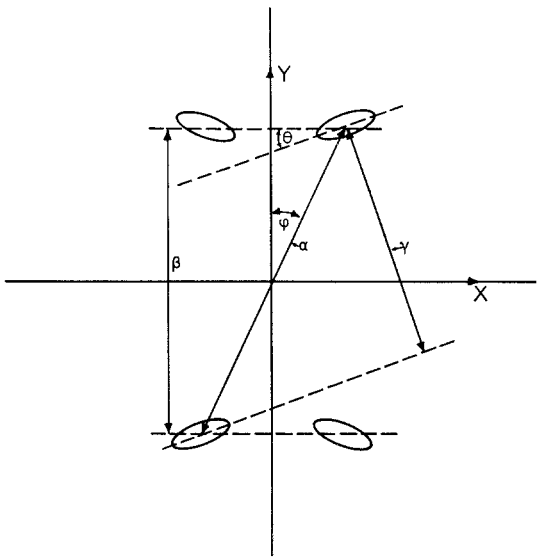

Figure 12 Diagrammatic representation of low-angle X-ray patterns in range 2 (e.g. see fig. 3) defining the quantities used in the text.

can be considered as lying on two sets of layer lines inclined to y, the inclination being equal to the rotation of the individual maxima towards y.

The split of the low-angle maxima about y (2ϕ in fig. 12) for the whole measurement series is plotted in fig. 13 as a function of annealing temperature; fig. 14 is a similar plot for the equatorial (x) split of the 200 wide-angle reflections shown before in part 1. To facilitate the comparison between the two, a plot was made of the sum of the two angular separations given by figs. 13 and 14 (fig. 15). This immediately reveals that, over a wide temperature range, this sum is constant, hence the increase in angular separation of the 200 reflections is exactly compensated by the decrease in separation of the low-angle reflections. It follows that the lamella rotates as a whole with unaltered structure. At 100° C, the constancy of the sum of the angular splits is lost; the low-angle reflections move faster towards y, until their final coalescence there at 105° C. This latter point, as we shall see, corresponds to a singularity in the entire behaviour pattern, and will be denoted by B (fig. 4 and table I).

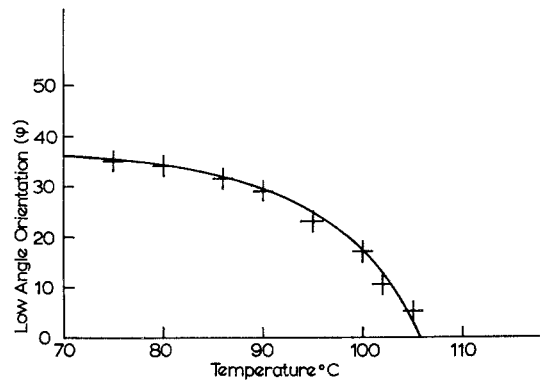

Figure 13 Variation of ϕ, the angle between the lamellar normal ($\mathbf{n}_L$) and y, with temperature.

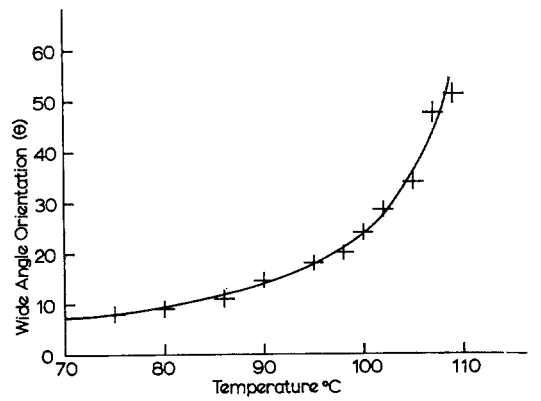

Figure 14 Variation of θ, the angle between the chains (**c**) and y, with temperature.

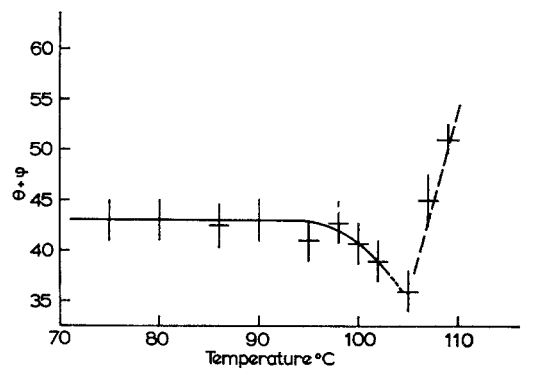

Figure 15 Variation of the sum of ϕ and θ, in figs. 13 and 14, with temperature.

Range 3 This range, between 105 and 108° C, is characterised by the fact that the low-angle maxima remain on y, although the 200 maxima in the wide-angle patterns keep splitting further

apart (fig. 5). This gives rise to the rapid upswing of the curve in fig. 15.

Range 4 Between 108 and 110° C, the character of the reflections changes abruptly, becoming more diffuse. Eventually, they reappear in a more definite form, essentially as an arc (fig. 7z) or four-point diagram (fig. 6z) centred on x, the latter with intensification at $\pm 45°$ to x. Fig. 6z shows a split pattern which in fact consists of radial streaks. There is continued rotation around **b** in the wide-angle pattern until the second single-crystal anologue, stage C, is reached (figs. 6pw and 7pw), corresponding to the low-angle patterns in figs. 6z or 7z.

Range 5 In this range beyond 110° C, the low-angle pole distribution gradually randomises around z just as the unit-cell does, inferred from the wide-angle patterns, leading to the specific case of stage D where the lamellar normals are perpendicular to z but completely random around it (figs. 8z and 8x). In this stage, the unit-cell is completely random about **b** and corresponds to the spherulitic fibril analogue (fig. 8pw and table I).

Range 6 At temperatures above 115° C, complete melting and random recrystallisation take place.

2.2.3. Changes in Spacing

Bragg's law will be used for defining the spacing, being aware of the fact that the justification of this procedure is debatable in the case of such comparatively poorly defined diffraction effects. However, the long-spacing values will be of little consequence for this work, we merely wish to assign a measure to the sequence of changes to be presented for the sake of completeness. There are three distances which can be measured on the photographs – α, β, and γ, defined in fig. 12. α is the distance of the maxima from the origin and is, therefore, a measure of the interplanar spacing d_α. γ is the separation between the layer lines defined by the oblique spreads in fig. 12, and β is the projection of the maxima on y. This latter will correspond to the layer-line separation if the lobes in fig. 12 are normal to y, but not otherwise. It may be erroneously identified as γ or even as α in the case of line collimation which smears out the pattern and obscures the orientation effect.

The changes in α, β, and γ, expressed as Bragg spacings d_α, d_β, and d_γ, respectively, are shown by fig. 16. The measurements refer to the same samples as were used for figs. 13, 14, and

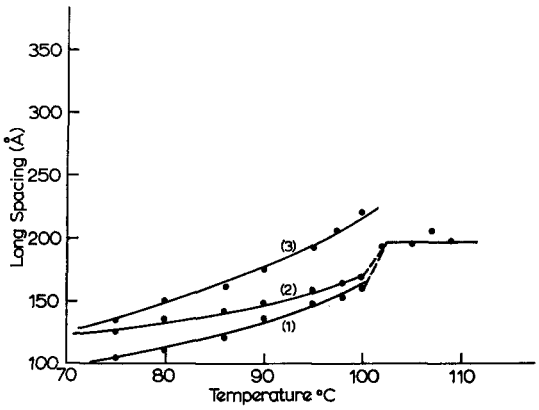

Figure 16 Variation of long period with temperature: (1) true lamellar periodicity (d_α); (2) periodicity along y (d_β); (3) layer-line periodicity (d_γ) (see text).

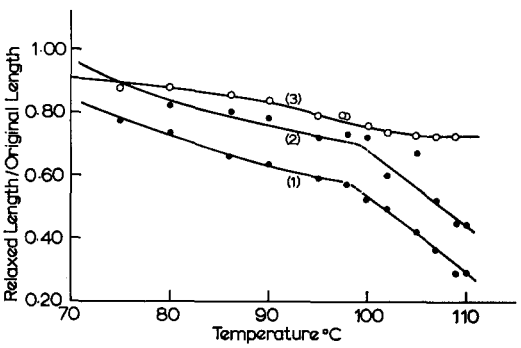

Figure 17 Variation of specimen length with temperature: (1) actual results; (2) anisotropic portion of change in length; (3) calculated curve for simple lamellar rotation around z.

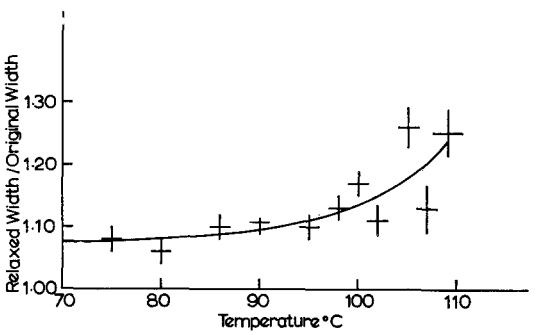

Figure 18 Variation of specimen width (z) with temperature.

15. Since the corresponding Bragg angles are small, d_α is inversely proportional to α and, from fig. 12,

$$d_\alpha = d_\beta \cos\phi = d_\gamma \cos(\phi + \theta)$$

From fig. 16, we see that d_α, the true lamellar

spacing, increases steadily up to 100° C, when there is a rapid, almost discontinuous, increase to an essentially constant value. This is the point at which the correlation between lamellar and molecular rotation is lost (fig. 15), ϕ becomes equal to zero and hence $d_\alpha = d_\beta$. At this point, also, it is no longer possible to recognise a layer-line character (fig. 4z); thus d_γ cannot be plotted beyond it.

2.3. Changes in Dimensions

Variations in length (y) and width (z) are plotted in figs. 17 and 18. Thickness changes (x) were not measured. There is a decrease in length by 20% and an increase in width by 7% on heating to 75° C. As density changes are inappreciable in this context, it is obvious, by inspection, that the increase in width is smaller than required by an isotropic increase of cross-section for the given shrinkage. In order to assess this departure from isotropy, we calculated the amount of contraction along y which would be associated with the *measured* increases in z, in case the zx section increased isotropically. Adding this amount to curve 1, curve 2, representing the anisotropic contraction, is obtained. We see that this still represents an appreciable amount of the total contraction. In fact the isotropic component of the y contraction (the difference between the ordinates of the curves 1 and 2) is practically constant, while the actual shrinkage along y increases with temperature. This means that a progressively larger portion of the contraction is becoming anisotropic. Beyond 100° C, the shrinkage becomes more pronounced, rather discontinuously, and the increases in width also become more appreciable. By 113° C, the initial specimen shape – that before drawing and rolling – was practically reconstituted.

2.4. X-ray Observations at the Relaxation Temperature

Both low- and wide-angle X-ray patterns were recorded at the relaxation temperatures themselves and compared with the diffraction patterns from the corresponding samples cooled to room temperature. In some cases, the temperature was raised and lowered successively to test for reversibility. With some samples, the low- and wide-angle patterns were recorded simultaneously, while in others, for instrumental reasons, different cameras were used for the two types of diffraction recording on different pieces cut from the same sample.

A representative selection of the results is included in table II and figs. 19 and 20. Further series where low- and wide-angle effects alone were examined fell in line with these results and will not be quoted separately. The effects are best grouped as follows.

Up to stage B A typical example is shown in table II, first row. The essential effect is the decreased value of 2ϕ (angular split of $\mathbf{n}_L$) in the low-angle diagrams, with an increasing split of the 200 reflections (2θ) in the wide-angle patterns at the elevated temperature. This means again that both the unit-cell and the lamellae rotate on heating and cooling, and that both these rotations are in the same sense. Both lattice and lamella orientation are further

TABLE II Reversible changes in orientation which occur on cooling from the relaxation temperature, for various temperatures (for definition of symbols see fig. 12).

Sample	Temperature (° C)	2θ (°)	2ϕ (°)	d_α (Å)	d_β (Å)
	95	42	49	135	148
In range 2	20	32	56	125	146
	95	41	49	136	149
At stage B	105	77	0	235	
	20	79	0	195	
In range 3	108	90	0	Streak along draw direction (y)	
	20	100	0	194 (Also weak random orientation)	
At stage C	110	90	0	Streak along draw direction (y)	
	20	180	—	Diffuse pattern more intense on x	

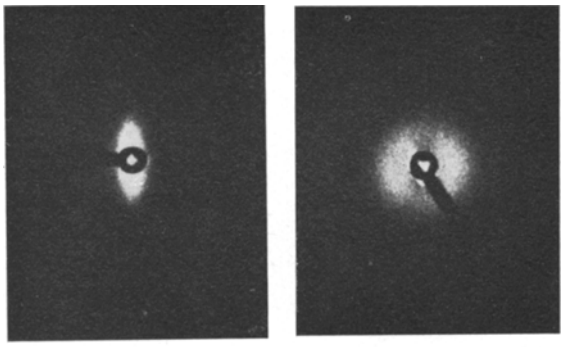

(a) (b)

Figure 19 Change in low-angle diffraction patterns between (a) annealing temperature, 109° C, and (b) room temperature. (X-rays along z; y vertical.)

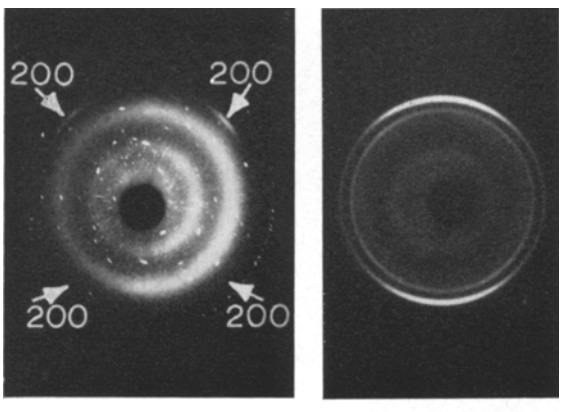

(a) (b)

Figure 20 Change in wide-angle X-ray diffraction pattern between (a) annealing temperature, 110° C, and (b) room temperature. (In (a) the sample is mostly molten, the remaining 200 reflections are indicated by arrows. The rest of the pattern is due to amorphous halo and the mica window of the hot stage.)

removed from the starting position of fig. 1; that is they correspond to a more advanced stage of annealing at the annealing temperature than at room temperature. The amounts of the two rotations are about identical; hence the inference that the lamella rotates as a whole, without change in chain orientation. Significantly, d_β remains constant; which in terms of the pattern means that the low-angle maxima move along lines perpendicular to y.

About stage B The rotations just described remain of the same magnitude until close to stage B. At stage B, this rotation suddenly ceases; both the low- and wide-angle diffraction patterns are unaffected by whether the photographs are taken at the annealing temperature or at room temperature, as far as orientation is concerned (second row of table II).

Beyond stage B The temperature invariance in the low-angle pattern orientation persists at stages beyond B. However, the reflections became radially streaked in the high-temperature photographs (fig. 19a). On further increase of the annealing temperature, this streak gradually contracts and eventually disappears. The corresponding room-temperature patterns, however, still follow the sequence laid out by figs. 5z-8z and table I (fig. 19b).

The behaviour of the wide-angle orientation, however, develops along a different pattern. Beyond stage B, there will be a difference again between the patterns taken cold and those taken at the annealing temperature. This difference, however, is the reverse of that observed at stages below B: with the beam along z, the 200 reflection is nearer to the equator, i.e. the unit-cell is in an orientation corresponding to a lower stage of annealing, in the photograph taken at the high temperature (e.g. fig. 20 and the third row of table II). In fact, when the high-temperature patterns alone are considered, the split of the 200 arcs, about the equator, increases only slightly with increasing annealing temperature, and the arcs never come near to y. The large splits of 200 about x and the eventual coalescing of the reflections on y, observed in the room-temperature photographs, along the annealing series in figs. $5p_W$-$8p_W$, develop essentially when the samples are cooled to room temperature. This is in agreement with early observations of Belbéoch and Guinier [7]. However, at this stage, another effect needs taking into account. All through the high-temperature series, the amorphous halo gains strength as the annealing temperature is progressively raised. This gradual melting effect becomes predominant at the stage now being discussed. The 200 intensification about y on cooling is associated with large amounts of amorphous material at the annealing temerature, hence with recrystallisation on cooling. As this behaviour would not be conveyed by entries in table II, an example is illustrated by figs. 20a and 20b. At the annealing temperature corresponding to stage C, the polymer is already predominantly molten, and, at that corresponding to stage D, melting is complete. Consequently, the spherulitic fibril structure in stage D is entirely the result of recrystallisation.

The following, further, significant effects were observed in the low-angle patterns at the elevated temperature.

(*a*) The spacing was always higher at the annealing temperature than at room temperature. Up to stage B, this is a direct consequence of the constancy of β (i.e. to the fact that the low-angle reflections move along lines perpendicular to y and not along circles). Beyond stage B, the effect is a pure spacing change without change in orientation. In case of higher annealing temperatures, the gradual contraction of the streaks is a manifestation of the same trend towards higher spacing at higher temperatures.

(*b*) The intensity of the low-angle reflections is always greater in the high-temperature photograph.

Effect of temperature-cycling Cycling the sample between the relaxation and room temperatures showed the small changes in orientation to be reversible over the complete range of temperatures. Similarly, the spacing and intensity changes were also reversible (e.g. see table II).

2.5. Redrawing Relaxed Specimens

2.5.1. Redrawing at Room Temperature

A sample relaxed at 100° C was redrawn progressively at room temperature to its original length. Initially, up to about 5%, there was an elastic range in which the wide- and low-angle patterns rotated together in a direction opposite to that observed on relaxation. The corresponding rotations amounted to 3 to 5°. Higher elongations produced permanent deformation. The wide-angle patterns continued to move towards the fully drawn pattern. The low-angle reflections, however, become weaker and more diffuse. A four-point pattern was still discernible, but superimposed on this was a diffuse reflection lying on y. This pattern was exemplified by the fully redrawn sample shown in fig. 21b. Here, the overall impression is a diffuse halo. However, closer inspection, more obviously when followed through the preceding stages, reveals that this in effect is composed of a four-point pattern, lying along layer lines perpendicular to y with spacing (d_α) equal to that of the relaxed sample (fig. 21a), and of a very diffuse spread, perpendicular to the draw direction, at a somewhat larger diffraction angle than the four-point reflections.

2.5.2. Redrawing at the Relaxation Temperature

In this case, specimens relaxed at 100° C (i.e. in a stage comparable to that in fig. 3) were redrawn at 100° C up to their original length. The wide- and low-angle patterns reoriented progressively over the full range of redrawing. The rotation in the wide-angle pattern was of the same magnitude but of opposite sense to that of the low-angle reflections. In fact, the original annealing sequence within range 2, table I, was reversed and the state in fig. 2 was reconstituted along the same route as it was left.

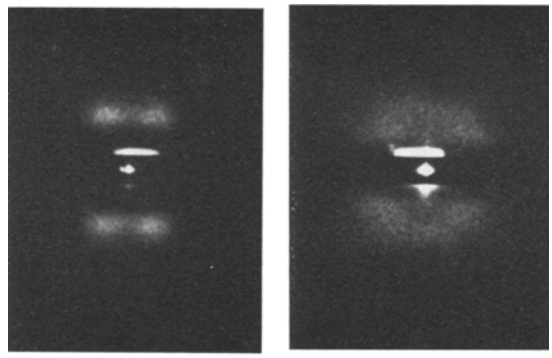

Figure 21 Change in low-angle diffraction pattern on redrawing: (a) sample relaxed at 100° C; (b) fully redrawn at room temperature. (X-rays along z; y vertical.)

Table III gives some details of the behaviour of the low-angle patterns in the course of this redrawing. The figures reflect the fact that the maximum moves round the corresponding Debye Scherrer ring – change in ϕ with unaltered spacing (d_α) – the spread along the oblique layer lines rotating with it (unaltered d_γ). The projection on y (d_β) will of course be affected.

The experiments were performed on samples both with and without cooling to room temperature before redrawing, with essentially identical results.

2.6. Relaxation at Constant Length

A single experiment was carried out by maintaining the sample at constant length during heat-treatment at 100° C, in association with the preceding experiment. The wide-angle patterns showed no change in unit-cell orientation; in fact a slight improvement of **c** orientation was just about indicated. Similarly, there was no change in the low-angle orientation. The spacing, however, did increase, but not as much as it did with the unconstrained specimen. The relevant figures are entered in the last row of table III.

TABLE III The effect on the low-angle diffraction of redrawing relaxed specimens (for definition of symbols see fig. 12).

	Sample treatment	Spacings (Å)			2ϕ (°)
		d_α	d_γ	d_β	
(A)	Relaxed at 100° C	132	188	152	62
(B)	(A) redrawn at 100° C (after cooling)	138	188	173	80
(C)	(A) redrawn at 100° C (no cooling)	140	201	173	79
(D)	Annealed at 100° C at constant length	116	164	148	80
(E)	Original sample	90	—	106	98

2.7. Observations on Fully Drawn Material

Samples which were fully redrawn at the relaxation temperature emphasised an effect which was found to be present in all drawn material. It was noted that, while under stress, the low-angle pattern showed a layer line truly normal to y (fig. 22b). Releasing the stress allowed the sample to relax slightly (10%) and the low-angle reflections were then found to be along tilted layer lines (see fig. 12). The slight (about 5°) effect is shown by fig. 22a. Wide-angle X-ray patterns showed a similar rotation of the 200 reflections. The effect was found to be reversible on restretching the sample (figs. 22a-22c).

The value of d_α is unaltered; however, it can be seen from fig. 22c that d_β, the projection on y, does change. Changes in long spacing with stress have been reported in both highly oriented polyethylene [8] and nylon [9]. In each case, however, d_β was measured, either by choice [9] or through employing slit collimation [8]. Our observations show that, in polyethylene at least, this need not correspond to an increase of lamellar periodicity.

2.8. Swelling

Representative samples of the annealing series were examined as regards dimensional changes on swelling in xylene. A precedent for such an examination was that by Point [3], to be referred to in the discussion. This part of our investigation is rather fragmentary. It consists of two measurement series and a few isolated observations. The first series was carried out by T. Kawai while in this laboratory. In this series, the samples were immersed in xylene at 30° C for several hours, the dimensions being measured with a low-power microscope while immersed in xylene but at room temperature. In the second series, carried out at a later date, the xylene was at ambient temperature all the time. The results are listed in table IV. Thickness measurements are not quoted, as the relative errors were too large to yield a meaningful trend. The orientation, shrinkage (etc.) parameters corresponding to the various entries in table IV can be read off from figs. 13-18 at the corresponding annealing temperatures. All swelling effects were reversible, the samples regained their initial dimensions on removal of the swelling agent.

Measurements on two additional samples not strictly part of the series will be quoted. One sample corresponded to stage C (**c** along x and **a** along y) and was thick enough along x

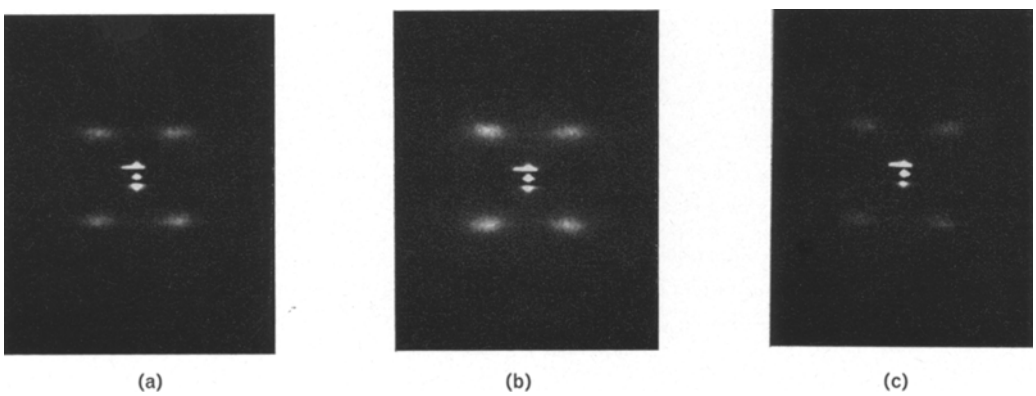

Figure 22 Changes in low-angle pattern after cold-drawing: (a) no stress; (b) stress applied (7% strain); (c) stress released. (X-rays along z; y vertical.)

TABLE IV The effect of xylene on the macroscopic dimensions of relaxed specimens.

Temperature of relaxation (° C)	Swelling (%)				Tilt of chains θ (°)
	Xylene (30° C)		Xylene (20° C)		
	Length y	Width z	Length y	Width z	
75	−2.0	~0	3.3	<1	8
86	4.8	~0	—	—	11
90	—	—	7.7	<1	15
95	—	—	7.6	<1	18
98	11.7	0.6	—	—	20
100	—	—	9.2	<1	24
102	—	—	9.2	<1	29
105	7.8	1.8	7.7	<1	34
107	7.2	1.8	8.8	0.6	47
109	—	—	7.3	—	51
116	4.8	1.7	5.9	6.3	Random

for this dimension to be measured. On swelling at 30° C, y increased by 7%, z by 0.8%, and x by 10%.

The second additional sample was drawn and rolled only and was swollen at 40° C in xylene, when the sample *contracted* along y by 5% and expanded appreciably along z (amount not placed on record). A control exposed to the same temperature in air showed no measurable dimensional change when examined at room temperature. On drying, slight further contraction occurred along y, adding up to a total reduction of 6.2%. On repeated swelling, there was an expansion of 1.2% along y (i.e. the dimension before drying was regained). This change of 1.2% proved to be reversible also on further drying and swelling. The initial 5% contraction, however, remained irreversible.

The sample annealed at 98° C (see table IV) was examined for low-angle X-ray scattering while in the swollen state. At this stage, the maxima have a split about y of 46°. The spacing was found to be 10% larger in the swollen than in the dry state, and changed reversibly with addition and removal of the swelling agent.

2.9. Selective Oxidation with Nitric Acid

Samples at various stages of annealing were exposed to oxidation-treatment with fuming nitric acid [10]. The treatment-temperature was generally 60° C, in some cases 70° C. The temperature only affected the time scale, not the nature of the effects observed.

A reorientation was manifest from the wide-angle patterns on strong enough nitric acid attack (e.g. after 40 h at 60° C). The orientation change was always of the type to bring the chain direction towards the original draw direction, y (i.e. it reverses the trend of the annealing process). This holds for all stages along the annealing sequence. Figs. 23 and 24 show diffraction patterns at two stages of annealing before and after nitric acid treatment. It will be seen that the split 200 reflections moved towards the equator by about 10° in both cases.

Low-angle patterns were affected differently by the nitric acid. At first they disappeared, but reappeared again after prolonged attack. The newly emerging pattern, however, was of different character than it had been originally. They formed along Debye Scherrer rings (and not layer-line streaks as before oxidation) with maximum intensity on y. Obviously, major changes in texture must have taken place, the explanation of which forms a separate line of work. Only the changes in the wide-angle patterns will be commented on in the discussion.

3. Discussion

The principal conclusions arise from the correlation of the orientation effects corresponding to the wide- and low-angle patterns. The wide-angle reflections from a known structure define the orientation of the unit-cell; the low-angle reflections define the magnitude and orientation of the structural units, which, as already stated, we identify with lamellae.

3.1. The Initial Lamellar Interface

The rather weak and diffuse layer-line streak with indefinite off-meridional intensifications is in agreement with general experience in drawn material and so is the intensification on slight annealing leading to stage A. The off-meridional

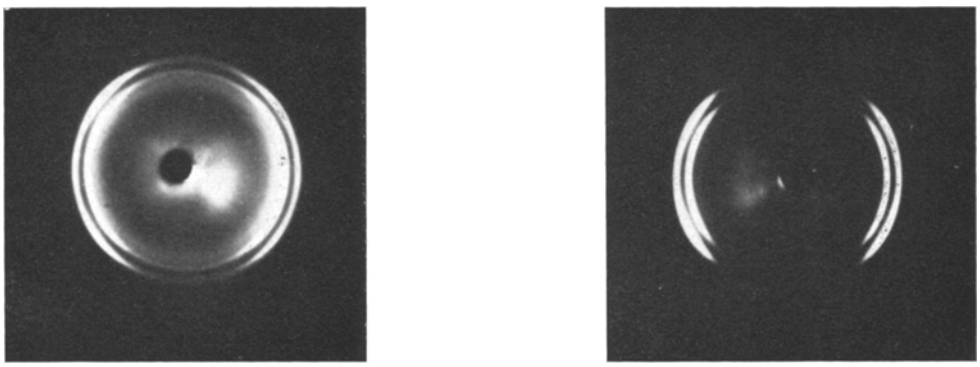

(a) (b)

Figure 23 The effect of nitric acid etching on wide-angle diffraction pattern: (a) relaxed at 105° C; (b) after 40 h at 60° in nitric acid. (X-rays along z; y vertical.)

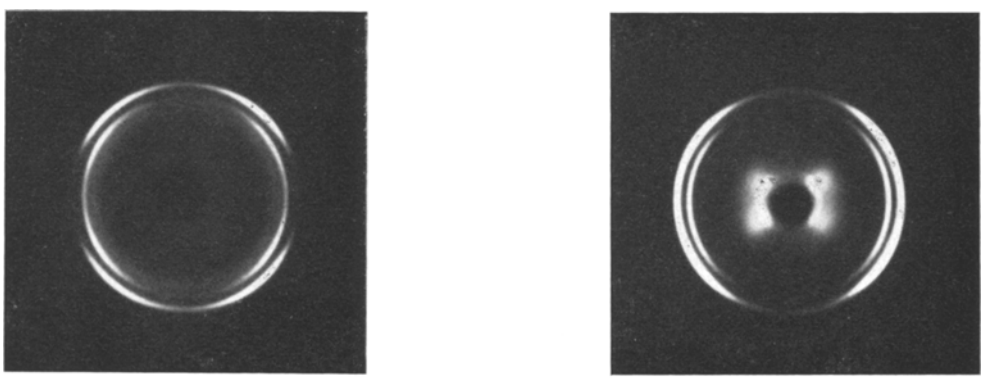

(a) (b)

Figure 24 The effect of nitric acid etching on wide-angle diffraction patterns: (a) relaxed at 108° C; (b) after 40 h at 60° C in nitric acid. (X-rays along z; y vertical.)

intensification has been attributed to oblique interfaces previously. However, the fact that in stage A we have the single-crystal analogue, where the crystallographic axes **a**, **b**, and **c** are uniquely defined with respect to the macroscopic dimensions of the specimen, now enables us to identify more uniquely the orientation of the texture element (lamella) with respect to the macroscopic sample and hence the crystal lattice. The experiment shows that the lamellar normal is in the xy plane, hence in the **ac** plane in terms of the lattice. This defines the lamellar interface as $(h0l)$ (i.e. lying parallel to **b**, hence z). The angle of near 45° between $\mathbf{n}_L$ and **c** identifies this interface as $\{301\}$.

Note It appears that Seto and Tajima [11] used samples of similar texture – obtained apparently accidentally – for their studies of macroscopic kink bands. Some of the texture changes observed by these authors, under more complex conditions of deformation, fall within the scheme to be presented here. Owing to the complexity of the experimental material, a more specific comparison would be too lengthy to be attempted here. We merely remark that parts of that paper are relevant to our argument.

3.2. Interlamellar and Intralamellar Slip

The distinguishing feature of range 2 (table I) is the rotation of $\mathbf{n}_L$. As seen from figs. 2-4 and 13-15, the two sets of lamellar normals rotate in opposite senses around z until they both become parallel to y at stage B, while the unit-cell rotates around **b** which stays parallel to z. The striking features of this rotation are that: (i) it is about a direction normal to $\mathbf{n}_L$ (hence parallel to the lamellar planes); (ii) the direction of rotation is such as to bring $\mathbf{n}_L$ to the original draw direction (y); (iii) the rotation stops when $\mathbf{n}_L$ is along y (see range 3). In addition, there is a simultaneous rotation of the wide- and low-angle plane-normals already

commented on. It follows, from the horizontal portion of the curve in fig. 15, that there are two sets of crystallites which must rotate bodily, in opposite senses, while the unit-cell orientation with respect to the crystallite is retained unaltered.

These observations are consistent with the behaviour of a stack of lamellae lying obliquely with respect to a compressive force (fig. 2m). The lamellae will slip past each other causing the whole stack to rotate until $\mathbf{n}_L$ is parallel to the force, when further slip, hence rotation, will cease (figs. 4m-5m). This process corresponds to interlamellar slip. The force required is compression along y. Tension would be expected to reverse the process, bringing $\mathbf{n}_L$ back towards the initial position (i.e. away from y). This in fact is observed on redrawing (fully at elevated temperature and partially at room temperature), consistent with interlamellar slip.

When $\mathbf{n}_L$ becomes parallel to the compressive force at stage B, interlamellar slip is expected to cease, in agreement with the observed invariance of the direction of $\mathbf{n}_L$ (figs. 4-5). The continued rotation of the unit-cell around **b**, hence z (figs. $4p_W$-$5p_W$), in range 3 must, therefore, increase the obliquity of the chains (i.e. the angle between **c** and $\mathbf{n}_L$) with respect to the basal planes of the crystals, causing plastic deformation of the crystal layer (figs. 4m-5m). This corresponds to intralamellar slip, again activated by compression along y, and is responsible for the final upswing of the curve in fig. 15.

The dip in the curve of fig. 15, *before* stage B is reached, is due to a rotation of $\mathbf{n}_L$ which is larger than that of the unit-cell (compare figs. 13-14). This corresponds to a reduction of the chain obliquity within the crystal (i.e. of the angle between **c** and $\mathbf{n}_L$) which is the opposite of the trend beyond stage B. The angle between **c** and $\mathbf{n}_L$ changes from 45 to 35°, which is equivalent to a transformation from {301} to {201} basal planes, representing a less oblique structure. Hence it appears that a crystallographic rearrangement occurs before stage B is reached (see later).

It is readily visualised that increasing intralamellar slip, beyond the stage in fig. 5, will lead to a gradual disruption of the crystal, which is in agreement with the blurring of the low-angle maxima. At this stage, however, melting and recrystallisation become pronounced; hence it is more profitable to consider this point separately.

3.3. On Oriented Recrystallisation

As judged from the increasing strength of the amorphous halo, melting occurs progressively as the annealing temperature is raised. If the fused material recrystallised in an unoriented fashion, we would obtain uniform diffraction rings superposed on the oriented pattern. This is *not* observed: at room temperature, we have an oriented texture only. This indicates oriented recrystallisation of the fused material. We can class effects in two groups, those up to stage B and those beyond it.

Up to stage B, melting effects are comparatively small. The fused material recrystallises in essentially the same orientation as the unmolten crystals (with the appropriate small reversible orientation change described in section 2.4, and to be discusssd). There are two possibilities. Firstly, whole crystalline regions melt, for reasons such as lower molecular weight, high branch content, or being highly stressed, and the randomised molecules crystallise again by attaching themselves to surviving crystals or nuclei, retaining the orientation of the latter. Secondly, it is possible that the crystals melt at the lamellar interface, melting spreading gradually along the straight stems towards the crystal interior. In this case, recrystallisation would occur by straightening of the disordered stem portions when the original crystal orientation would be automatically retained. Premelting of this kind is receiving much consideration (e.g. reference 12). The increased intensity of the low-angle reflections at elevated temperatures is being invoked as support for such melting at the layer surface [12]. Such intensity increase has in fact been observed also in the course of the present experiments (section 2.4).

Beyond stage B, melting becomes prominant, and much of the effects observed cold have arisen through recrystallisation. As described in section 2.4, on cooling, the chains move away from y (i.e. to an orientation corresponding to a higher stage of annealing). This orientation change could be due to the different orientation of the recrystallised material which is now in predominance, rather than to the reorientation of the crystallites already present, the latter representing only a tail in the orientation distribution at room temperature.

By the time stage C is reached, there is only little crystallinity left at the annealing temperature, and the room-temperature diffraction is largely due to recrystallisation. A pattern

with **a** parallel to, and **c** perpendicular to y would be expected from compression along y (see part 1 [1] – considering also **c** slip, if to begin with **c** is not perpendicular to the compressive force). Accordingly, stage C could result from crystallisation under compression. The existence of a compressive force along y is in line with all the preceding arguments. However, this is not adequate to account for the observed maintenance of **b** along z. For this, we have to assume that we have nuclei left in the melt in orientation appropriate to stage C. This does not obviate the need for a compression along y, but represents an additional requirement. In the absence of a compression, the next stage of relaxation, stage D, will result (see below).

The identity of the texture in stage D with that along a spherulite radius has been recognised by Point [3] (see part 1 [1]). The important new recognition at present is that stage D is the result of a primary crystallisation from the melt, which makes its relation to spherulite texture readily understandable. However, to keep all spherulite radii aligned along z, we have to impose spatial restrictions on the spherulitic development. Such would be the closeness of nuclei preventing spherulite growth in all directions except z (e.g. sheets of nuclei perpendicular to z). In addition, if nuclei retained a preferred orientation in the melt, with **b** along z, a spherulitic fibril growth along z will be promoted. However, some spatial restrictions, in the form of adjacent centres, would still be required to prevent the divergence of the growing crystal by the usual sheaving process.

Orientation produced by closeness of nuclei has a well-documented precedent in crystallisation under stress. In that case, the existence of nucleating threads, which may consist of extended chain crystals, forming under stress was inferred. It is possible that a similar factor is at play in the present case, extended chain threads of higher thermal stability having been formed during the original orientation process. This possibility has already been elaborated elsewhere [13] and is being examined at present [4]. The feasibility of such a picture is being indicated by work now in progress.

3.4. Some Comments on Redrawing

It is encouraging that interlamellar slip can be reversed by drawing. This indentifies at least one important structural effect in the course of drawing. Further, in contrast to the annealing experiments, the appropriate structural change can in this case be produced isothermally with externally controlled forces. This opens up the possibility of assessing the energetics of the processes quantitatively. Conversely, it should enable the evaluation of the corresponding load/extension curves in terms of known structural changes, one of the main objectives of mechanical studies. Full reversibility over the whole orientation range is possible only at or near the annealing temperature. It is encouraging, nevertheless, that reversible interlamellar slip could also be identified at room temperature even if only over a small extension range (larger extensions undoubtedly involve disruption of the crystals). The fact that the phenomenon in question can be identified with the elastic range of the deformation of our samples suggests that interlamellar slip could be an important, if not the representative, process of the elastic region of the deformation behaviour in semicrystalline polymers.

3.5. Long-Spacing Increase

As seen from fig. 16, the long spacing increases throughout the annealing sequence. Nevertheless, it appears that the orientation sequence just discussed is unaffected by the actual value of the long period (i.e. as if the orientation and crystal thickening processes were unrelated effects). The following facts support this contention. In the case of linear polyethylene, large changes in the long period can be produced without appreciably altering the initial **c** orientation. In the present work on low-density polyethylene, we found (section 2.6) that orientation changes on annealing could be prevented by keeping the sample at fixed length. At the same time, however, the long spacing does increase, even if to a lesser extent than it would do under similar conditions when free. Also, the dimensional changes seem to be largely unaffected by the actual values of the long spacings, which has interesting implications to be discussed later. It appears therefore that long-period changes are of no consequence for the present discussion.

One feature, however, needs at least a comment, namely that the spacing changes reversibly on cycling between annealing and room temperature. In range 2, this effect is coordinated with a well-defined orientation effect and is, apparently, the consequence of the maintenance of a fixed periodicity along y, hence it appears

to be due to some still-unclarified geometric constraint in the structure (sections 2.4 and 3.8). This does not apply to stage B and beyond, where the reversible spacing change is not associated with orientation effects. We have no structural conception as to what such reversible spacing changes are due. They have been observed in a more pronounced form recently in polyoxymethylene [14].

3.6. Shrinkage

The orientation process on annealing is associated with reduction of length. The interlamellar slip, in range 2, in itself is expected to lead to a decrease in the dimension of the stack along y. Consider a system with lamellae of thickness l with normals at an angle ϕ_1 to y. The length of a lamellae along y will be $l_1 = l \cos \phi_1$. If the lamellae now rotate to ϕ_2, then $l_2 = l \cos \phi_2$. Thus the specimen length along y should change in the ratio

$$l_2/l_1 = \cos \phi_2/\cos \phi_1$$

Taking l as the initial sample length along y and obtaining values for ϕ from the X-ray patterns, l_2/l_1 is plotted in fig. 17. It is seen that the length decrease is much too small to account for the observed sample shrinkage. However, we have seen that the observed shrinkage can be expressed as a sum of isotropic and anisotropic portions. Isotropic contraction is predominant at the early stage of the annealing sequence. With increasing annealing temperature, the contraction becomes more anisotropic, the isotropic portion of the total dimensional change remaining essentially constant. It is to be expected that dimensional changes associated with lamellar rotation will be anisotropic (see below). If, therefore, we compare the calculated curve with the curve representing the anisotropic portion of the total contraction in fig. 17, we see that the agreement is reasonable. Accordingly, we have identified at least one portion of the total contraction with lamellar rotation, hence with interlamellar slip.

The suggestion that the initial contraction is mainly isotropic, and is not related to the crystallite rotation, agrees with the birefringence observations reported in part 1 (reference 1, fig. 12). Here it was shown that the birefringence dropped more rapidly initially than could be accounted for from crystallite rotation. This was attributed to changes occurring in the amorphous orientation. Such changes would be expected to have transverse isotropy.

3.7. Support for the Lamellar Model from Subsidiary Evidence

3.7.1. Obliquity Analogy with Known Lamellar Structures

As stated, $\mathbf{n}_L$ is always perpendicular to the **b** crystal axis, which means that the corresponding planes are $\{h0l\}$. This points to an immediate tie-up with unoriented systems of known lamellar texture where the basal planes are $\{h0l\}$, such as the unoriented, melt-crystallised bulk consisting of layers with predominantly {201} (or {101} for low crystallisation temperatures) basal planes [15]. Further, solution-grown crystals with 100 prism faces have {201} basal planes in the appropriate (100) sectors or, in the case of highly elongated crystals, in the entire crystal layer [16, 17]. We see that there is a unifying feature which is common to the simplest monolayer crystals from dilute solution, to the unoriented bulk, and to the oriented material.

The reason for {301} surfaces in the early stages of annealing and their transformation to {201} at stage B may be as follows. According to the example of unoriented systems, {201} is the basal plane which forms on spontaneous crystallsation at low supercoolings. Consequently, the more oblique {301} interface in the oriented systems would correspond to a higher energy configuration imposed by the stresses of the original orientation process. When these stresses relax sufficiently at the appropriate stage of annealing, the crystals may take up the same {201} obliquity they would have possessed in the absence of orientation initially, even if such a transformation in the given crystal orientation is in opposition to the general trend of moving the **c** axes further away from the original draw direction. It is noteworthy that there is a discontinuity in all curves representing different properties (figs. 13-17) at the temperature where this obliquity transformation starts.

3.7.2. Dimensional Changes

On shrinkage The anistropy of the contraction on annealing in range 2, where lamellar rotation is inferred, has already been commented on. In spite of the appreciable shrinkage along y, the z dimension is only slightly affected. This is consistent with rotation of lamellae with $\{h0l\}$

surfaces around **b** (i.e. *z*). In addition, the amount of anistropic contraction along *y* corresponds to that expected from lamellar rotation, as commented on earlier. This correspondence is the more remarkable as the rotation occurs simultaneously with an increase of the long spacing (fig. 16). This suggests that variation in the long-spacing values leave the sample dimensions unaffected. At first sight, this appears surprising, as one might expect an increase of sample dimension along **c** associated with an increase of the long period. That this need not be so in the case of chain-folded lamellae is demonstrated by the behaviour of solution-grown crystals. It has been observed [18, 19] that mats obtained by sedimenting single crystals from suspensions do not change their dimensions as the fold length of the component crystals increases. In particular, oriented mats with **c** along the mat-normal, obtained by oriented sedimentation of crystal layers, do not change their thickness on refolding to greater fold length. Undoubtedly, a given individual layer does thicken. The constancy of the mat thickness must therefore mean that the layers can slide past each other freely as they contract laterally on thickening. In this way, the gaps left behind by any one contracting layer will be filled by other layers moving in laterally. Therefore, the crystals will be redistributed with unaltered macroscopic sample shape. The individual layers will be thicker, but there will be correspondingly fewer layers across the thickness of the mat, leaving the total mat thickness unaffected. Although, to our knowledge, never commented on previously, this mass redistribution by sliding of lamellae must be considered as a definitive fact in the case of single-crystal lamellae. As the corresponding dimensional invariance is now inferred in the oriented bulk, the same explanation suggests itself also in this case. Note that this analogy would imply the existence of chain-folded lamellae which slide past each other with appreciable freedom.

On swelling More specific information on the role played by the textural elements comes from the swelling experiments (section 2.8). There is a definitive correlation between the increase of specimen dimensions and the orientation of the long spacings, which is consistent with a picture that the effect of the swelling agent is, essentially, to increase reversibly the lamellar periodicity, the overall sample dimensions being affected accordingly. In structural terms, this means that the swelling agent either separates the layers or that it increases the thickness, but not the width, of the amorphous interface between the crystalline portions. The increase in lamellar periodicity on swelling has been directly confirmed by the increase in the low-angle X-ray spacing in a sample in range 2. It is remarkable that the change in X-ray spacing agrees practically quantitatively with the increase of the corresponding sample dimension. To our knowledge, this is the first time that such a correspondence could be demonstrated.

The following principal observations are consistent with the above picture and were utilised in making these deductions: practical absence of expansion along *z* and sizeable expansion along *y* throughout the whole series. The expansion along *y* appeared to be largest in stage B and was comparable along *x* and *y* in stage C (in the only case where thickness changes could be measured reliably). None of these effects would follow from consideration of molecular orientation alone. In fact, expansion along *y* in the unannealed, or only slightly annealed, samples appears paradoxical from traditional considerations, as it corresponds to expansion along the draw direction in what is essentially a **c**-axis oriented system.

In such a system, traditionally, a contraction is to be expected on swelling, as it would involve the randomisation of stretched amorphous material tying together the oriented crystallites. Indeed, such irreversible contraction was observed by us at slightly increased temperatures. Undoubtedly, this is related to the isotropic contraction, associated with the initial stages of annealing, occurring in the absence of swelling agent at higher temperatures. The effect of swelling is probably to increase the mobility of the molecules and thus to decrease the temperature at which irreversible shrinkage can take place. But even this shrinkage is superposed on a reversible swelling extension, which makes itself apparent as soon as the irreversible contraction effect is removed. The additional contraction on drying, and the expansion comparable to this additional contraction on repeated swelling (section 2.8) are manifestations of the reversible effects which we associate with variation in lamellar separation.

The invariance along *z* at stage D has been noted earlier by Point [3], before lamellar structures had been recognised. Point's early

observation, together with the whole series presented here now, follows readily from our picture of the lamellar texture and lends further support to the model.

3.8. On the Forces Acting; the Nature of the Amorphous Material

The most obvious consequence of annealing is the shrinkage of the sample, which as we have shown is in excess to what would follow from the geometry of crystal rotation. This points to a retracting force along the original draw direction, the source of which must lie outside the crystal lattice proper. Thus this force could exert the compression on the crystals along y invoked to account for our reorientation effects. This force must be due to stored energy which is created in the course of the original orientation process, and which becomes gradually released on increasing the temperature.

For the argument to follow, consider a stage within range 2, say the one in fig. 3m. Here the crystal rotation has reached a certain stage and has stopped. For further rotation, the temperature needs raising. There can be two causes why interlamellar slip should cease at a given stage. The first is simply geometrical: there will be a gradually decreasing force component along the interlamellar slip plane as the crystal rotates from fig. 2m to fig. 3m. Even when the friction, resisting the slip, is constant, this resistance will at some stage balance the diminishing driving force and bring the slip, and hence rotation, to a halt. This factor will always be operative. In addition, the resistance to slip may increase due to stored energy building up in the course of slip.

The existence of restoring forces is indicated by spontaneous alignment of the **c** axes towards y under two kinds of experimental conditions: (i) on nitric acid treatment (section 2.9); (ii) on cooling the sample from the annealing temperature to room temperature (section 2.4). The analysis of both cases is complicated by the fact that we are producing structural changes within the material by the experiment itself. Nevertheless, the effect of a reversal towards the more highly oriented state is remarkable, as in no obvious picture is an improved, overall chain alignment expected without externally applied force. Elastically stored energy opposing crystal rotation would account for it if we envisaged that, under the conditions in question, the balance, between the forces which activate the slip and those which resist it, is disturbed in such a way as to reduce the former.

Nitric acid treatment Nitric acid is known to cut and remove amorphous material and folds, leaving paraffin-type layers behind [20]. However, an aggregate of paraffinoid crystals would either fall apart or, if it cohered, would retain the crystals in the original orientation within the fibre. Such an aggregate would not reorient itself. Accordingly, reorientation must occur before all ties between crystals are removed. There is no reason why indiscriminate removal should change the crystal orientation. If, however, the amorphous material causing the slip were preferentially attacked, then the equilibrium state between slip-producing and slip-resisting forces would be shifted and the observed reorientation would result. This argument is based on wide-angle observations alone (see section 2.9). The low-angle reflections, observable only in the final stages when presumably all amorphous and fold material is removed, correspond to a different type of texture, which bears probably little relation to the stage at which the effects in question occur.

Reversible changes with temperature It is notable that reversible changes with temperature hold throughout range 2 but cease at stage B (i.e. when interlamellar slip should come to an end). One could take the viewpoint that, in first approximation, the structure is unaffected by the temperature; but that the temperature coefficients of the two kinds of elastic elements (i.e. slip-producing and slip-resisting) are different (e.g. this could happen if the mobility of the molecules responsible for promoting slip were reduced to a larger extent). On the other hand, it has been shown that some recrystallisation occurs on cooling, and melting on heating, when cycling between the annealing and room temperatures, even if within range 2 these effects are not as dominant as they become in higher ranges. This phase transformation may, therefore, be the source of the reversibility. If the molecules, responsible for producing the slip, crystallised to a larger extent on cooling than the ones opposing slip, the observed overall trend would again be explained. In fact, the two effects in this paragraph would be inseparable.

Phase changes involving crystallisation and melting of the crystal interface – which as already mentioned are a possibility now widely studied – would create a special situation. If the crystals melted gradually, from the interface

inwards, the chain portions in the newly molten regions would tend to randomise; hence their length (end-to-end distance) would be reduced as compared to their extended state in the crystal. On the other hand, the chains would require greater volume in the amorphous phase, while, at the same time, the overall lateral extension of the amorphous phase would be confined to the unaltered cross-section of the crystal, with which it remains in molecular continuity. Clearly this situation raises many complex problems on the nature of such possible pre-melting phenomena, which we shall not discuss here, besides recognising the fact that they may need noting. One effect, nevertheless, will be pointed out. As stated in section 2.4, the low-angle reflections move along lines perpendicular to y on temperature-cycling. In the first place, this means that spacing and orientation both change, the spacing being smaller at low temperatures, an effect not accountable by rotation of unaltered crystals alone. Secondly, the constancy of d_β (table II) means that orientation and spacing changes are coordinated, so that a textural periodicity along y (i.e. the original draw direction) remains constant irrespective of molecular orientation. We shall not comment on the possible sources of this periodicity, as morphological studies are in progress which promise to throw light on this significant effect.

The forces acting are long-range and elastic, hence they must reside in amorphous material. The slip-producing compressive force must be the one associated with shrinkage and, in analogy with stretching and contracting of rubber, must be produced by chains stretched during the original drawing process. They either remain in the amorphous state, but are prevented from contracting by viscous forces at room temperature, or, alternatively, they may become parts of stress-induced crystals which may melt first as the temperature is raised. On the other hand, the slip-resisting forces would need to be ties between crystal layers, which become increasingly stretched as adjacent crystals are displaced. Possible melting/recrystallisation behaviour at the crystal interface would have a pronounced influence, both for geometrical reasons, by affecting the space requirement of the lamellae, and for energetic reasons, by producing and removing entropy elastic material in specific relation to the crystals.

Whatever the definitive molecular picture, the present considerations show that any unifying concept of amorphous material is oversimplified. Distinction is required between different kinds of amorphous material according to the forces to which they give rise. Ultimately, these differences must all be attributable to the particular relation of a given amorphous segment to the crystal morphology (e.g. whether it is a stretched-out part from a disrupted crystal or whether it belongs to a crystal interface as a loose loop or an intercrystalline tie, etc.). There is no simple approach to this problem. Here we merely tried to present some symptoms indicative of such distinctions.

3.9. On the Nature of the Crystals

The lamellar nature of the crystals, while not a rigorous consequence of the X-ray effects, seems to tie up with all our own observations and with existing knowledge. Many further questions could be asked as regards (*a*) the arrangement of these lamellae and (*b*) their molecular structure.

(*a*) The questions are: what is the lateral extension of the lamellae, how many lamellae form a coherent stack which shears via inter-lamellar slip, and what is the relation between the constituents of a double texture as in fig. 2m? We do not attempt to speculate on these points here as direct morphological work is in progress [4].

(*b*) In many respects, there is an analogy with systems with established chain-folded structure, such as the lamellar morphology in itself and the type of obliquity involved. In chain-folded crystals, the obliquity was attributed to the packing requirement (staggering) of the folds. As far as similar effects suggest similar causes, this in itself suggests chain-folding in the present structures. In addition, the remarkable individuality displayed by the lamellae is noteworthy. They can slip past each other and they can be separated by swelling. This indicates at least as much that the layers are not fully interconnected (each stem in one layer, with another stem in the next), which implies a certain amount of folding-back of the chains. The amount of folds in relation to traversing molecules, however, remains uncertain.

All these considerations referred to stage A and beyond. The morphology of the cold-drawn (and rolled) sample, as such, is likely to be less well-defined, in view of the lower intensity and definition of the low-angle pattern. This is in keeping with existing ideas, according to which

the lamellar structure only develops on annealing, by either extended chains folding up [23] or chain-folded regions, disrupted by drawing, coalescing [21, 22]. Whichever the case, the structure after cold-drawing is highly strained. Heat-treatment gives it a chance to organise, leading to morphologically better-defined entities.

3.10. Summary of the Relaxation Process

We start with the cold-oriented material. Here the textural entities are poorly defined and we have locked-in stresses. On slight annealing, which does not change the overall crystal orientation, some stresses are relaxed, causing shrinkage and allowing an improved organisation of the submicroscopic texture. This leads to the formation of lamellae with oblique {301} interfaces at 45° both to the molecules and to the draw direction. On increasing the temperature further, compressive stresses acting along the draw direction are released. The maximum resolved shear stress due to this compression will lie along the lamellar interface and perpendicular to **b** (and none along the molecules in the lattice), which will cause interlamellar slip, producing crystal rotation around **b**. At any stage of rotation, the slip-activating compression will be in equilibrium with slip-resisting elastic forces (tie molecules ?) generated by the slip. When the crystal layers become perpendicular to the draw direction, further rotation ceases because there is no further component of the compressive force along the lamellar interface. However, at this stage, the {100} planes within the crystal will be most favourably oriented for slip along **c**, which will now take over, representing intralamellar slip, hence plastic deformation, and eventual disruption of the crystals, until the molecules become all perpendicular to the draw direction. At these stages, progressively increasing melting takes place at the annealing temperature, and recrystallisation on cooling. This recrystallisation is oriented. In the first stages, it seems to be influenced by the compressive forces still present. At more advanced stages of annealing, the recrystallisation is essentially that from an unoriented melt, the resulting orientation being due to restriction imposed by the closeness and possible orientation of surviving crystal nuclei. The whole sequence of events is accompanied by a gradual increase of lamellar thickness. Changes in crystal obliquities (e.g. transformation from {301} to {201} basal planes) also occur.

4. Concluding Remarks

The range of structural effects which become apparent promise to point beyond the confines of the rather special phenomena investigated here. The system chosen for this investigation had the particular advantage of spreading the effects involved over a large temperature range, which made them amenable for detailed study. This is no doubt due to the comparatively large amorphous content in the branched material. While the most high crystalline linear substances are more advantageous for the study of the crystal morphology as such, the less crystalline Alkathene is more suited for the examination of phenomena which depend on the interplay between amorphous material and the crystals on which, after all, much of the characteristic and desired properties of polymers depend.

Acknowledgements

Acknowledgement is made to the Ministry of Technology who supported this work.

We also acknowledge the contribution of Dr T. Kawai who carried out the series of swelling measurements referred to in the text and who prepared several specimens, in the early stages of this work, while in our laboratory. Our thanks are due to Professor F. C. Frank for numerous helpful discussions.

References

1. I. L. HAY and A. KELLER, *J. Matls. Sci.* **1** (1966) 41.
2. A. BROWN, *J. Appl. Phys.* **20** (1949) 552.
3. J. J. POINT, *Memoires et Publications de la Société des Science des Arts et des Lettres du Hainaut* **71** (1958) 65.
4. N. B. CRYER and A. KELLER, to be published.
5. A. FRANKS, *Brit. J. Appl. Phys.* **9** (1958) 349.
6. P. H. MEIBOHM and A. F. SMITH, *J. Polymer Sci.* 7 (1951) 449.
7. B. BELBÉOCH and A. GUINIER, *Makromol. Chem.* **31** (1959) 1.
8. A. I. SLUTSKER, T. P. SANPHIROVA, A. A. YASTREBINSKII, and V. C. KUKSENKO, *IUPAC Symposium*, Prague (1965), Preprint No. P. 536; *J. Polymer Sci.* **C16** (1967), in press.
9. D. R. BERESFORD and H. BEVAN, *Polymer* **5** (1964) 247.
10. I. L. HAY and A. KELLER, *Nature* **204** (1964) 862.
11. T. SETO and Y. TAJIMA, *Japanese J. Appl. Phys.* **5** (1966) 534.

12. Y. NUKUSHINA, Y. ITOH, and E. W. FISCHER, *Polymer Letters* **3** (1965) 383.
13. A. KELLER and M. MACHIN, *J. Macromol. Sci. (Phys.)* **B1** (1967) 41.
14. K. O'LEARY and P. H. GEIL, *ibid*, p. 147.
15. A. KELLER and S. SAWADA, *Makromol. Chem.* **74** (1964) 190.
16. T. KAWAI and A. KELLER, *Phil. Mag.* **11** (1965) 114.
17. H. D. KEITH, *J. Polymer Sci.* **A2** (1964) 4339.
18. A. KELLER, unpublished work.
19. W. O. STATTON and P. H. GEIL, *J. Appl. Polymer Sci.* **3** (1960) 357.
20. R. P. PALMER and A. J. COBBOLD, *Makromol. Chem.* **74** (1964) 174.
21. A. PETERLIN, *J. Polymer Sci.* **C15** (1966) 427.
22. E. W. FISCHER and H. GODDAR, *IUPAC Symposium*, Prague (1965), Preprint P.558; *J. Polymer Sci.* **C16** (1967), in press.
23. P. F. DISMORE and W. O. STATTON, *J. Polymer Sci.* **C13** (1966) 133.